Numerical investigation of hydrodynamic and mixing conditions in a torus photobioreactor

Jeremy Pruvost, L. Pottier, Jack Legrand

Numerical investigation of hydrodynamic and mixing conditions in a torus photobioreactor

J. Pruvost*, L. Pottier, J. Legrand

Université de Nantes, CNRS, GEPEA UMR–CNRS 6144, Bd de l'Université, CRTT – BP 406, 44602 Saint-Nazaire Cedex, France

Abstract

It is well-known that the response of photosynthetic microorganisms in photobioreactor (PBR) is greatly influenced by the geometry of the process, and its cultivation parameters. The design of an adapted PBR requires understanding of the coupling between the biological response and the environmental conditions applied. Cells culture under well-defined conditions are thus of primary interest. A particular lab-scale PBR has been developed for this purpose. It is based on a torus shape, that enables light to be highly controlled while providing a very efficient mixing, especially along the light gradient in the culture, that it is known to be a key-parameter in PBR running. A complete characterization of hydrodynamic conditions is presented, using computational fluids dynamics (CFD). After validation by comparison with experimental measurements, a parametric study is conducted to characterize important hydrodynamics features with respect to PBR application (light access, circulation velocity, global shear-stress), and then to investigate a possible optimization of the process via modification of the impeller used for culture mixing. The final part of the study is devoted to a detailed investigation of mixing performance of the torus PBR, by numerically predicting dispersion of a passive tracer in various configurations. The high degree of mixing observed shows the great potential of such innovative geometry in the field of photosynthetic microorganisms cultivation, especially for the design of a lab-scale process to conduct experiments under well-controlled conditions (light and flow) for modeling purpose.

Keywords: Mixing; Simulation; Hydrodynamics; Torus photobioreactor; Microalgae; Dispersion

1. Introduction

Photosynthetic microorganisms like microalgae and cyanobacteria have a high potential in various areas, including food (as feed for larvae and juveniles of bivalve molluscs), pharmacology (bioactive molecules, toxins), cosmetics (pigments), environment (CO_2 removal, wastewater treatment) and even energy production (H_2). But, despite this well-known potential, examples of industrial valorizations remain scarce, and are mainly restricted to particular applications, like biomass or pigments production in mass culture (Lorenz and Cysewski, 2000; Olaizola, 2003). Difficulty of proposing adapted processes, called photobioreactors (PBR), that permits to reach sufficient productivity, is mainly explained by the complex interaction between the photosynthetic microorganisms growth and culture conditions. Preliminary investigations in a fully characterized process, where all pertinent parameters can be controlled with high accuracy, are thus of primary interest. By this way, culture parameters can be first optimized at the lab-scale, including a modeling approach, and an adapted industrial sized PBR with economic feasibility can next be proposed in a second time.

Many examples of PBRs are found in literature (Pulz, 2001; Tredici and Materassi, 1992) but generally developed for particular applications. There are only few examples of geometries for fundamentals studies under well-defined conditions (Cornet et al., 1994, 1998; Csogör et al., 1999; Hoekema et al., 2002; Wu and Merchuk, 2001). Whatever is the application, light reveals to be the major factor controlling, and often limiting, the productivity of bioprocess involving photosynthetic microorganisms (Richmond, 2004). Because of the cell concentration, light is highly absorbed and diffused when crossing the culture (Cornet et al., 1998; Csogör et al., 2001). This leads to

* Corresponding author. Tel.: +33 2 40172668; fax: +33 2 40172618.
E-mail address: jeremy.pruvost@univ-nantes.fr (J. Pruvost).

an heterogeneous radiation-field, that prevents light to be considered as a common substrate, like mineral nutrients for example, where a homogeneous concentration can often be supposed in a first assumption (well-mixed reactor). To relate the light supply to the culture growth, light attenuation in the biological turbid medium must be accurately described. This determination is not trivial, and is highly correlated to the PBR geometry (Cornet et al., 1998). Analytical and accurate solutions are facilitated if the one-dimensional hypothesis on the radiation-field can be done, i.e., light attenuation occurs in a unique main direction, perpendicular to the illuminated face of the PBR (Cornet et al., 1995, 1998). For more complex geometries, numerical resolution of the radiative transfer equations has to be performed, but it is time-consuming, reducing interest in the field of a fully controlled process definition, where various parameters can be modified easily. This explains why most of PBRs, especially those involved in fundamental studies and modeling, are naturally designed under the one-dimensional hypothesis, like rectangular geometries with an incident perpendicular radiation-field (Chini Zitelli et al., 2000; Cornet and Albiol, 2000; Hoekema et al., 2002), cylindrical ones with external radial illumination (Cornet et al., 1998), or annular ones with internal radial illumination (Muller-Feuga et al., 2003a; Ogbonna et al., 1996).

A second important parameter is the hydrodynamics applied in the geometry. The culture must be sufficiently mixed to prevent flowing cells from sedimentation and to homogenize nutrients concentration. But, it is indeed known from an experimental basis that hydrodynamics can have additional complex effects on photosynthetic microorganisms (Muller-Feuga et al., 2003a,b; Richmond, 2004; Wu and Merchuk, 2002). This influence can be related to two different reasons, that are the shear-stress effect on living cells, and the homogenization of the light received per cell. The first one is a common problem encountered in all cell-sensitive cultures, as with mammalian cells for example (Curran and Black, 2004; Elias et al., 1995), but despite its apparent simplicity, shear-stress effect on living medium is very difficult to fundamentally investigate (Ghadge et al., 2005; Pruvost et al., 2004b). It is indeed well-known that some species are especially sensitive to the mechanical shear that appears in a disturbed flow, and the mixing can then be in extreme cases the critical parameter of the application (Barbosa et al., 2004; Sanchez Miron et al., 2003; Wu and Merchuk, 2002). But how to characterize and formulate effects of shear-stress on a living cell is still a problem to solve. From a physical point of view, mechanical effects of a given hydrodynamics on a particle (a living cell in this case) can be of various forms (Ghadge et al., 2005), including the different components of the shear-stress tensor as well as pressure gradients, and their respective time variation if the flow is turbulent. From the biological point of view, cell response to shear-stress is highly related to the species considered, and can be of various natures, ranging from an alteration of the physiological behavior to the cell alteration and destruction (Jaouen et al., 1999). These responses are certainly a function of the shear-intensity, its nature and the time of exposition to a particular intensity. This complexity explains why effects of shear-stress on a living medium (and especially for photosynthetic microorganisms) remain rather unknown, and thus uncontrolled.

In contrary to the shear-stress, effects of mixing on the light received by each cell of the overall population is specific to the photosynthetic microorganisms (Wu and Merchuk, 2001, 2002). Indeed, because of the heterogeneous radiation-field in the photobiorector, each cell receives instantaneously a specific amount of light. It is thus important to generate hydrodynamic conditions that promote mixing along the light gradient so as to homogenize light received by each cell with respect to time. Each individual cell will have a behavior representative of the global culture, and the modeling of the biological response will then be performed more easily, using standard growth models applied on the overall biomass. Such approach is usually conducted in PBR modeling, but it must be noticed that it implies a well-mixed assumption of the culture with respect to the light gradient. If not the case, difference in residence time in different depths of culture will lead to a non-negligible influence of flow conditions (Cornet et al., 2003; Luo and Al-Dahhan, 2004; Pruvost et al., 2002). It must be added that, for certain species, a second possible effect can result from an intensive mixing along the light gradient, that makes photosynthetic microorganisms subjected to light intensity variations in PBR. This is especially the so-called light/dark cycles effects, as observed in many studies (Grobbelaar et al., 1996; Janssen et al., 1999; Lee and Lee, 2001; Merchuk et al., 1998). Influence of such a phenomenon on PBR performance remains, as for shear-stress, rather misunderstood. Light regime in PBR is indeed complex and can only be characterized if those light–dark cycles effects are known, that implies light attenuation and cells trajectory to be both determined, each being a physics complex problem (on its own). Assuming a radiative model is available, cells trajectory can be obtained by, for example, radioactive particle tracking (Luo et al., 2003), or with a Lagrangian approach (Muller-Feuga et al., 2003b; Pruvost et al., 2002). For the last one, the flow-field must be well-determined in the all geometry. The light regime finally obtained has then to be linked to the physiological response, that is another delicate problem considering its complexity (Cornet et al., 2003; Janssen et al., 1999; Luo and Al-Dahhan, 2004, Pruvost et al., 2002).

In this study, a laboratory-scale PBR designed to conduct cultures under well-defined and controlled conditions is presented and investigated. In addition to classical bioreactor controls like pH or temperature, the set-up allows a simple and accurate determination of the light received by the culture, while providing good mixing conditions. To satisfy both conditions, the PBR presents flat surface and an internal torus shape (Fig. 1(a)). Light transfer aspect in such geometry has been treated elsewhere (Pottier et al., 2005), and the assumption of the one-dimensional hypothesis for radiative transfer modeling was especially verified. This study is especially focused on hydrodynamic aspects. With regard to mixing, some studies have shown interest of loop configurations like torus shape reactors, but in the field of biochemical applications like enzymatic reactions (Legrand et al., 1997; Nouri et al., 1997), or heterogeneous liquid–liquid reaction (Tanaka and O'Shima, 1988). A high dispersion is attained, because of Dean vortices

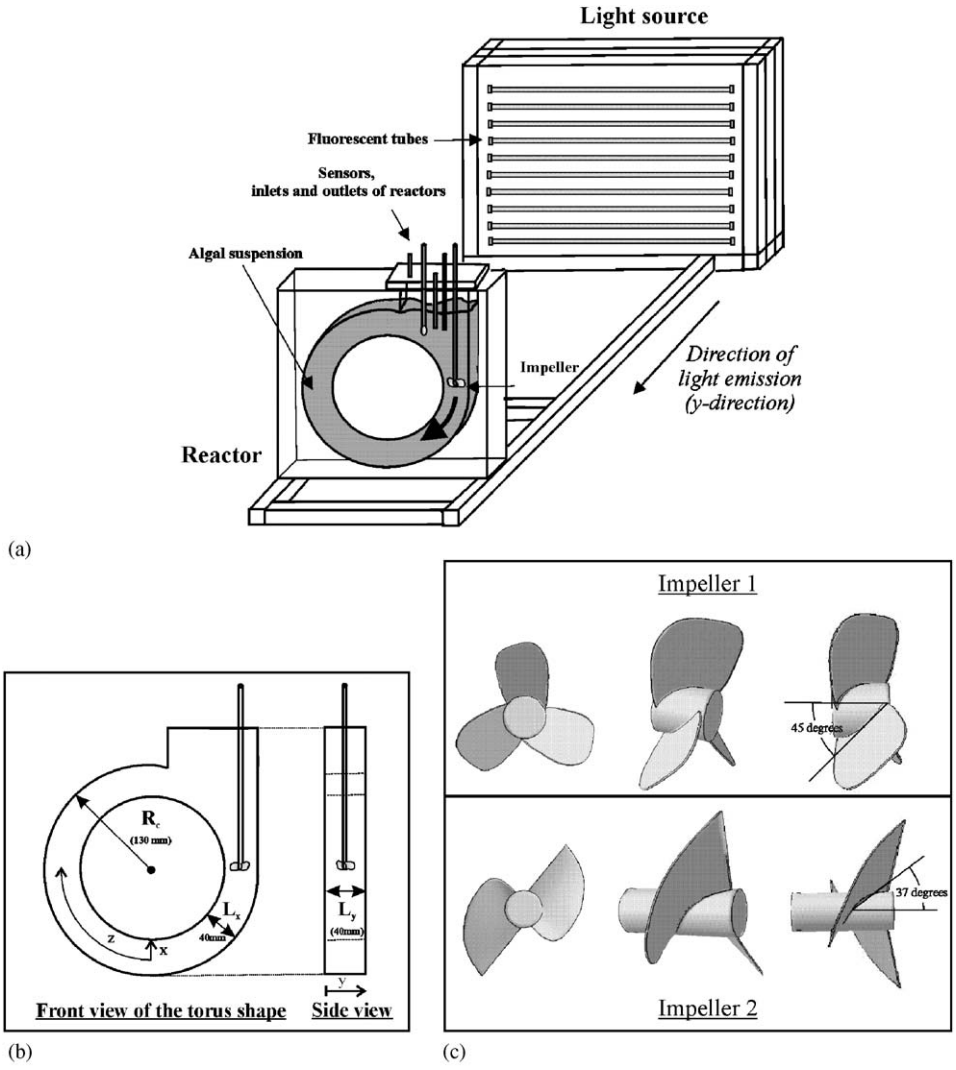

Fig. 1. Schematic representation of the torus photobioreactor and of both impellers investigated.

generated by the reactor bends, and of the rotation of the marine impeller that generates a three-dimensional swirling motion in the geometry (Pruvost et al., 2004c). The combination of these two effects leads to an absence of dead volumes in the reactor. Torus reactors appear thus as an interesting alternative to classical cylindrical stirred tanks usually employed in mixing applications. For microalgae culture, and especially if reactors of high efficiency are needed, tank geometries are not suitable because of a limited surface to volume ratio compared to flat geometries. By combination with good mixing conditions, the proposed torus PBR allows a large illumination front surface for a given culture volume, that makes it interesting for preliminary laboratory investigations. One possible drawback of such a geometry is the eventual shear-stress field that is not perfectly controlled (but it is also the case in stirred tanks), and remains heterogeneous, as in the impeller region, where relative high shear-stress can be achieved. But, the loop configuration of the torus geometry has theoretically two advantages. The first is that the recirculation in the loop implies the entire culture to cross the impeller region at each new revolution in the geometry, and thus all cells are subjected to undergo an almost identical history with respect to shear-stress. This will facilitate the understanding of the global response of the culture to shear-stress generated in the geometry. The second advantage of the loop configuration is that low impeller rotation speeds generally allow an efficient mixing. It is thus expected that in such geometries, shear-stress will be kept sufficiently low to prevent from adverse effects on the culture.

In any case, to relate with accuracy process parameters to the biological response, conditions in the PBR need to be well-defined. To characterize hydrodynamics as a function of operating parameters in the torus shape PBR, computational fluids dynamics (CFD) will be employed. Such a tool has been successfully applied and validated on a reactor of almost similar geometry, but not devoted to photosynthetic microorganisms culture (Pruvost et al., 2004c). Major characteristics of flow in torus geometries were emphasized, especially the competition of Dean vortices that appear when an axial flow occurs in bends, with the solid-body rotation involved by the swirl flow generated by the impeller rotation. Because of the decay of the

swirl intensity with the distance from the impeller, competition between both phenomena evolves in the geometry, resulting in non-established flow conditions with respect to the axial direction. It was especially shown that highest swirl motion was not achieved at higher impeller rotation speed. Under low rotation speeds of the impeller, due to the reduction of the axial pumping effect of the impeller and its influence on Dean vortices appearance, the swirl flow maintains further away in the reactor.

In this study, mixing conditions are especially investigated with respect to photosynthetic microorganisms application. After validating the numerical modeling of the PBR with experimental measurements obtained using particle image velocimetry (PIV), a complete numerical study is conducted and results for two types of impeller at various rotation speeds are presented. Some global values are defined to focus on the PBR application, by linking flow conditions to cells sedimentation, light access, shear-stress, etc. Next, by solving numerical dispersion of a passive tracer in unsteady state, performance of the reactor is investigated in term of mixing time. Finally, lateral dispersion in the reactor was characterized using a steady-state resolution of tracer dispersion. Combined with flow structure visualization, it allows a detailed study of the movement generated along the light attenuation, emphasizing interest of the torus PBR to generate effective light access conditions.

2. Photobioreactor description

The PBR is presented in Fig. 1(a). Illuminated surface of $0.0325\,m^2$ is of torus shape with an external radius $R_c = 0.13\,m$, the length L_z of the loop being 0.82 m (Fig. 1(b)). The reactor is managed in PMMA (polymethyl methacrylate) and is thus fully transparent. To prevent from optical distortion and to avoid curved surface perpendicular to the emitting direction of the light source, the front surface is plane, and the torus channel is square-sectioned with a gap width $L_x = L_y = 0.040\,m$, leading to a reactor volume of 1.31 (Fig. 1(b)). The light supply is placed in front of the geometry, light emission direction being perpendicular to the illuminated surface of the reactor (Fig. 1(a)). By this way, light attenuation in the depth of culture (along y-distance) can be considered monodirectional, allowing simple light transfer models to be applied in further investigation of the radiative-field in the PBR (Pottier et al., 2005). The culture is circulated by the rotation of a marine impeller. The PBR can receive a complete loop of common sensors and automations for microalgae culture, namely, temperature, pH, dissolved oxygen concentration and gas injection (CO_2 and N_2). Because no measurements are presented using microalgae culture, this reactor part will not be described.

Two types of marine impeller have been used in this study (Fig. 1(c)), both having same diameters of 0.036 m. The first is of classical type (impeller 1), with three flat blades and a blade pitch angle of 45°. The second is especially shaped for axial pumping (model S215 "high efficiency propeller", Prather—http://www.pratherproducts.com), with two curved blades and a blade pitch angle of 37° (impeller 2). The rotation speed can be ranged from 0 up to 1000 rpm, and is measured using an optical tachymeter. Both impellers are shown in Fig. 1(c).

3. Hydrodynamics characterization

3.1. Numerical prediction

3.1.1. Mesh consideration

A similar approach is conducted as already described in details in Pruvost et al. (2004c) for the simulation of another torus geometry using FLUENT software (Fluent Inc). Only main characteristics are presented in this study. The torus shape is three-dimensionally meshed using the GAMBIT software (Fluent Inc). The resulting grid is shown in Fig. 2. Because of the complex geometry of both impellers, hybrid meshes are retained, with an irregular zone composed of tetrahedral volumes and prisms in the impeller region, and a regular mesh with elementary hexahedral volumes elsewhere. In the irregular part, cells density is refined as going closer to the impeller. Pruvost et al. (2004c) have investigated effect of the near-wall consideration for torus reactor simulation. The standard approach with application of a wall-function based on the universal logarithmic profile (standard wall-function) was found to give satisfactory results, in accordance with experimental measurements. Despite an improvement can be expected with an approach involving a full resolution of momentum equations in the boundary layer like with a low-Re model, the great increase in grid refinement in the near-wall region, and thus in time computing, was not found to be justified, only a slight difference being observed between both approaches (Pruvost et al., 2004c). A standard wall-function approach is thus retained in this study, with an adequate meshing in the wall region.

The resulting grid is composed of 738 896 cells. A coarsened mesh (308 115 cells) was defined to test grid independency. Example of results are given in Table 1 ($N = 400$ rpm, impeller 2), for the mean bulk velocity U_0 and for the mean value of turbulent kinetic energy k averaged on the entire reactor volume. Because only a slight difference is observed between both predictions, the finest mesh was retained for further investigation.

3.1.2. Turbulence model, boundary conditions and numerical details

A k–ω model (Wilcox, 1998) was used for turbulence modeling. This model was found in Pruvost et al. (2004c) to give the most accurate prediction by using the commercial code FLUENT in the case of torus shape reactor simulation. The torus reactor is of closed type, and thus no inlet or outlet flow conditions are applied. The flow results from the impeller rotation which is the only driving mechanism. Such a case can be modeled using a multiple reference frames (MRF) resolution. Solution is achieved by solving the equations of motion in two different reference frames, one being the absolute inertial frame, the other attached to the impeller being in rotation with a rotation velocity equal to that of the impeller. Full description of the method can be found in Brucato et al. (1998), and its application to torus geometry in Pruvost et al. (2004c). The only boundary condition to be specified is the rotation

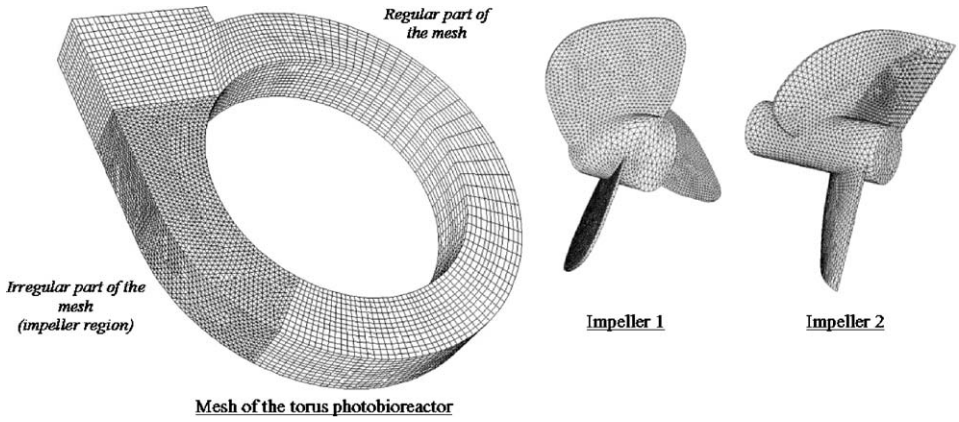

Fig. 2. Mesh topology.

Table 1
Examples of grid independence tests ($N = 400$ rpm, impeller 2)—mean bulk velocity U_0 and mean turbulent kinetic energy $\langle k \rangle$ averaged on the entire reactor volume

	U_0 (m s^{-1})	$\langle k \rangle / U_0^2$
Finest mesh (738 896 cells)	0.1633	0.0096
Coarsened mesh (308 115 cells)	0.1649	0.0090

velocity of the impeller. In order to facilitate the convergence to the steady-state flow, the rotational velocity of the impeller is increased in two successive steps. An intermediate converged solution corresponding to the lower speed of rotation investigated (100 rpm) is next used to initialize hydrodynamic values for higher rotation velocities.

A second order interpolation scheme was applied for all discretized transport equations (pressure, momentum and turbulent characteristics). Momentum and turbulence equations were numerically solved using a segregated method, that implies to solve the pressure–velocity coupling with an iterative correction procedure "SIMPLEC". Computations were performed until convergence of all residual criteria was found (no variation). For all flow-field resolutions, default constants of the turbulent models retained in FLUENT were employed and a steady-state calculation was made.

3.2. Particle image velocimetry (PIV) investigation

In order to validate numerical predictions, flow conditions in the PBR were experimentally investigated. Because of the set-up transparency that allows optical access and of the square-sectioned internal duct that prevents from optical distortion, the PIV method is well-suited. The set-up is presented in Fig. 3. The PIV system used is marketed by Dantec (FlowMap system), and it consists of a Nd:Yag laser, a CCD camera with a definition of 768×489 pixels and Flowmanager software for analysis. Results for the axial component U of mean velocity are presented in Fig. 4 for an acquisition area located at a distance from the impeller $z/L_z = 0.75$, and for $N = 900$ rpm.

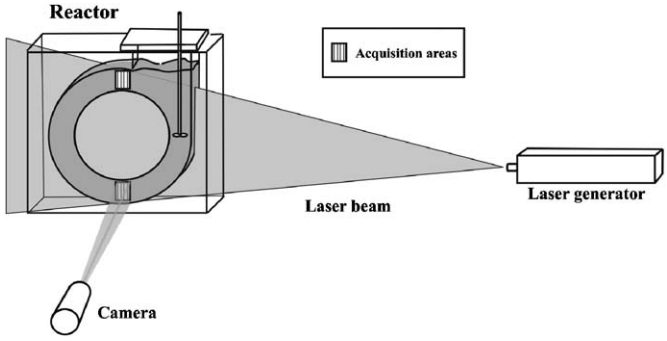

Fig. 3. Sketch of the experimental set-up for PIV measurements.

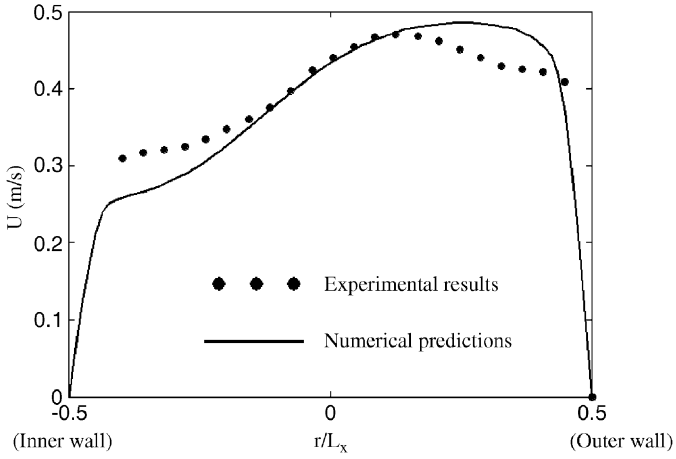

Fig. 4. Comparison between predicted and measured axial mean velocities ($N = 900$ rpm, impeller 2, $Z_{imp} = 0.75$).

Relative agreement is observed between numerical prediction and experimental measurements. The order of magnitude of axial velocity is well-predicted, as well as the particular evolution of its profile. For position far from the impeller, centrifugal force induced by the bend configuration shifts the maximum velocity towards the outer part of the bend curvature. But it can be noticed that a small difference between experimental and

numerical results near walls (error calculation gives a mean deviation of 5.6% between experimental measurements and numerical prediction, with a maximum value of 15.3% near wall). Considering that accuracy of PIV measurements decreases slightly in the wall vicinity (which is in the order of magnitude of errors stated), this is, however, difficult to conclude on the numerical calculation relevance in this region (choice of the near-wall treatment, isotropy of turbulence assumed in k–ω model...). The numerical procedure described in the previous section was thus retained.

4. Results

4.1. Global characterization of hydrodynamics characteristics of the torus PBR

The first part of the numerical investigation is devoted to a global characterization of hydrodynamic conditions in the torus PBR as a function of the impeller speed and shape, in the scope of microorganisms cultivation. Hydrodynamic values linked to cells suspension, light access and shear-stress were thus especially considered. In the torus geometry, cells suspension is achieved if a minimum mean bulk velocity U_0 is applied. Light access given by cells trajectories along the radiation-field is a more complex function of hydrodynamic conditions. In a first assumption, it can be supposed to be roughly a function of the average value of the velocity component V_y along the light gradient (lateral velocity), in this case in y-direction (Fig. 1), and of the mixing due to turbulence, characterized by turbulent kinetic energy k. Because same conclusions have been achieved with both criteria, only results for the lateral velocity V_y are presented. To facilitate comparison between different conditions, local values of lateral velocity V_y have been averaged in the entire reactor volume. Averaged values are denoted by $\langle\,\rangle$ in figures.

As for the light access, the shear-stress applied to living cells is difficult to characterize in details. In a first assumption, it can be related to the strain rate ε deduced from the rate-of-deformation tensor S as follows:

$$\varepsilon = \sqrt{\sum_{ij}(S_{ij}S_{ij})} \quad \text{with } S_{ij} = \left(\frac{\partial U_i}{\partial x_j} + \frac{\partial U_j}{\partial x_i}\right). \tag{1}$$

Two global values $\langle\varepsilon\rangle$ and $\langle\varepsilon_{\text{imp}}\rangle$ were again defined. They represent stain rate intensities averaged on the total volume of the PBR and in the impeller region, respectively (impeller region is shown in Fig. 2). It is evident that only some trends can be accessed using such characterization (the resulting shear-stress field is evidently heterogeneous and, for example, effects of the turbulent motion on shear-stress fluctuation is not considered in the definition).

Results for the mean bulk velocity U_0 as a function of the impeller rotation speed are given in Fig. 5. Those results are compared to the correlation proposed by Khalid and Legrand (2001), which was established in a torus reactor, but with circular section. The mean bulk velocity obtained for a given impeller rotation speed is even lower in the case under study.

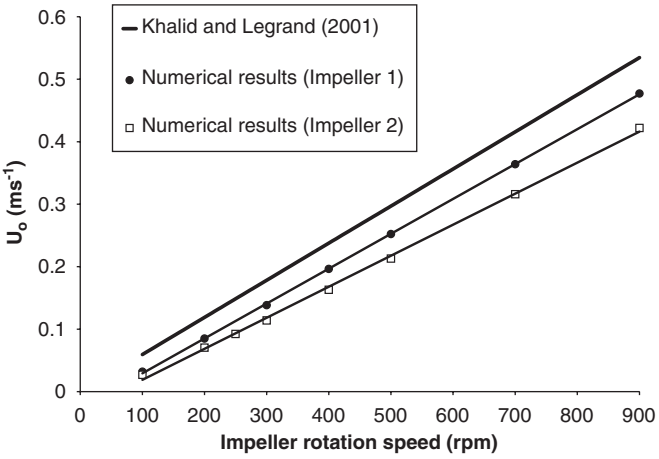

Fig. 5. Predicted mean bulk velocities U_0 as a function of the impeller rotation speed (dots: numerical results; lines: best fit).

The use of a square-sectioned geometry reduces thus the induced flow rate in the torus geometry (around 10–20%, considering results in Fig. 5). This result was expected, because a swirl type flow is better maintained in circular-sectioned pipes. Considering that only small values of U_0 are needed to prevent cell sedimentation, this loss of efficiency is acceptable for our PBR application. If results obtained between the two impellers are compared, a slight decrease in efficiency is observed with impeller 2 (15% compared to impeller 1), despite such an impeller being theoretically better shaped for axial pumping. This is certainly explained by the number of blades and the resulting surface of pumping, higher in the impeller 1 case. The special shape of impeller 2 does not compensate for the difference in pumping surface with impeller 1. Finally, it must be noticed that all relations between mean bulk velocities and impeller rotation speeds are strictly linear (in agreement with correlation of Khalid and Legrand, 2001). Such a linear evolution will facilitate practical utilization of the PBR, to correlate cells sedimentation for a given microorganism species to a minimum mean bulk velocity (for example, experimental observation with a cultivation of *Chlamydomonas reinhardtii* in the torus PBR gives U_0 around 0.05 m s^{-1}).

Fig. 6 shows evolution of the average component of velocity $\langle V_y\rangle$ along the direction of the light attenuation in the PBR (i.e., y-direction), and the shear-stress criteria $\langle\varepsilon\rangle$ and $\langle\varepsilon_{\text{imp}}\rangle$, as a function of the mean bulk velocity U_0. For all values, an almost linear evolution is still observed. Considering results for $\langle V_y\rangle$, due to the rotating axial flow generated by impeller of marine type, increasing the bulk velocity results in a more intensive movement along y-direction. Significant values of the lateral velocity component are obtained (around 10% of the mean bulk velocity), which is interesting for PBR application (efficient mixing along the direction of light attenuation). Impeller 1 appears again to give better results for a given bulk velocity (40–60% increase). If results for shear-stress are considered, both impellers result in an almost similar mean shear-stress obtained in the entire reactor values (values of $\langle\varepsilon\rangle$). This is not the case for values calculated in the impeller region

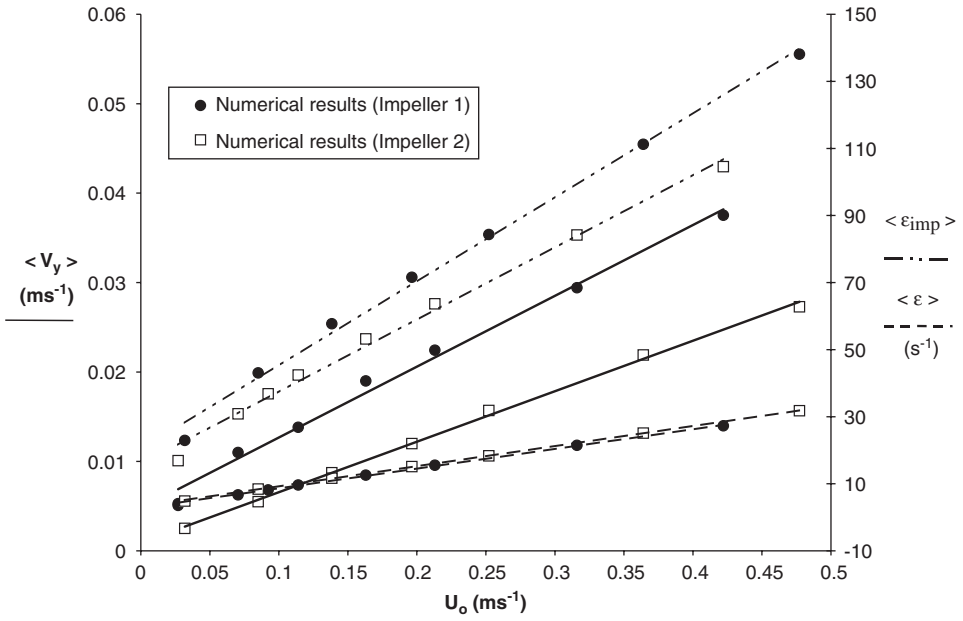

Fig. 6. Predicted global values $\langle V_y \rangle$ and $\langle \varepsilon \rangle$ as a function of the mean bulk velocity U_0 (dots: numerical results; lines: best fit).

(location of high shear-stress), a significant local increase being observed with impeller 1 (30–40%).

This primary investigation permits to draw some interesting conclusions, as for example the interest in impeller 1 (three-blades marine impeller) if species cultivated tolerate the shear-stress achieved in the impeller region. For a given flow rate applied in the PBR, a more efficient movement is induced along the light penetration depth. The linear evolutions of mean relevant hydrodynamic characteristics with respect to the impeller rotation speed is another interesting feature. This simplifies adjustment of hydrodynamic conditions. For example, the operating domain for a given species cultivation in the torus PBR can be determined by setting a minimum value of U_0 to prevent from sedimentation, and a maximum value of $\langle \varepsilon \rangle$ to remain below cells sensitivity (or $\langle \varepsilon_{\text{imp}} \rangle$, depending on the value found relevant to characterize shear-stress effect on living cells, i.e., maximum or mean value of the shear-stress). In this domain, the mixing along the light gradient can then be adjusted. Influence of conditions on photosynthetic growth can be next simply investigated.

4.2. Detailed investigation of mixing in the torus PBR

To complete the preliminary investigation of operating conditions in the torus PBR (mean bulk velocity, light access, global shear-stress), it appears interesting to further investigate the mixing in the geometry. The investigation can be divided into two parts. The first deals with the characterization of the mixing time, as usually used in stirred tanks studies, and the second is devoted to a detailed determination of the mixing along a single revolution in the torus geometry. Both parts are based on the determination of the transport of a passive tracer, which is easy to numerically conduct.

The passive tracer was chosen with same physical properties as the continuous phase (water). In turbulent flows, the diffusion process has to consider the turbulent mass diffusivity D_{jt}, expressed in a turbulent Schmidt number, relating turbulent mass diffusivity to the local value of the turbulent viscosity μ_t in the reactor. The turbulent Schmidt number is defined by

$$Sc_t = \frac{\mu_t}{\rho D_{jt}}. \tag{2}$$

In turbulent regime, the mass transport equation to solve is

$$\frac{\partial C_j}{\partial t} + \vec{V}\,\vec{\text{grad}} C_j = (D_j + D_{jt})\nabla^2 C_j, \tag{3}$$

where D_j is the usual mass diffusion coefficient obtained in laminar regime ($D_j = 2 \times 10^{-9}\,\text{m}^2\,\text{s}^{-1}$ for a passive tracer in water), and C_j the concentration of the passive tracer. This transport equation is implemented in Fluent, and values of μ_t are obtained from the k–ω model. Only the turbulent Schmidt number value has to be defined to calculate D_{jt} in Eq. (3). It was set to $Sc_t = 1$ (Bird et al., 2002). A discretization scheme of second order was used for the resolution of the mass transport equation. Depending on the purpose of the study (see further for details), the resolution was conducted in steady or unsteady state. It must be noticed that in this part, only Eq. (3) was solved. Because a passive tracer is used, there is no influence of mass transport equation on the flow field, and thus, results of the flow-field obtained in the global characterization of the reactor with the steady-state resolution of momentum and turbulent equations are still valid in Eq. (3).

Dispersion studies were done for impeller rotation speeds leading to turbulent regime, determined by calculating the corresponding Reynolds number using the mean bulk velocity U_0 predicted before ($Re = \rho U_0 L_y/\mu$).

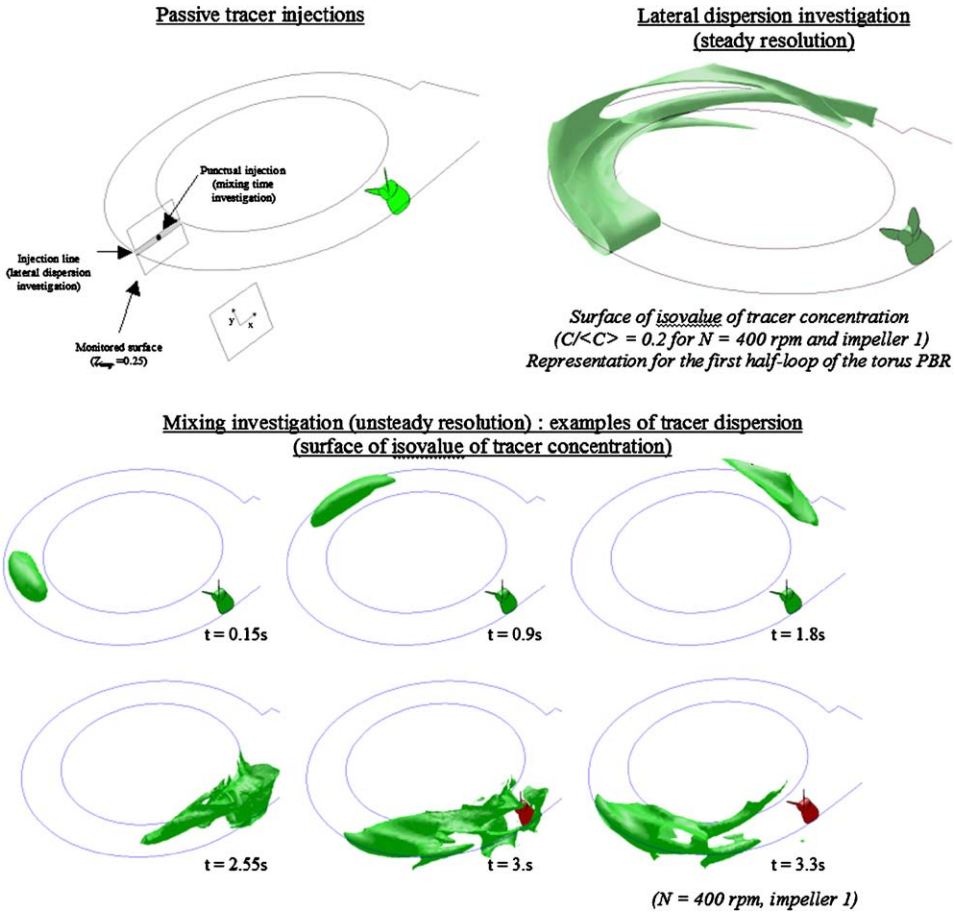

Fig. 7. Dispersion numerical investigation: locations of injections and examples of results.

4.2.1. Mixing performance of the torus reactor

Mixing performances were first evaluated by numerically determining the mixing time in the torus PBR. To evaluate it, a punctual tracer injection of pulse type was simulated. Mixing time was determined by the time evolution of the average tracer concentration on a given flow cross-section. The injection was located in the same flow cross-section as the monitored surface, at a distance $Z_{\text{imp}} = z/L_z = 0.25$ from the impeller (as shown in Fig. 7). To determine the tracer dispersion in the PBR, an unsteady resolution was carried out. For each case simulated, it was verified that the time step was sufficiently small to not influence the dispersion calculation. Influence of the time step was determined by performing different resolutions, as presented in Fig. 8. This example (impeller 2, $N = 500$ rpm) shows clearly that a time step smaller than 0.01 s does not influence the time resolution (deviation on predicted values of mixing time between $\Delta t = 0.01$ s and $\Delta t = 0.005$ s being below 0.5%). This procedure was repeated for each case presented.

An example of a complete dispersion resolution is given in Fig. 9 (impeller 2, $N = 400$ rpm). The tracer concentration averaged on the monitored surface was normalized by the concentration obtained when a total dilution was achieved (final homogeneous concentration $\langle C \rangle$). Mixing time was determined by the time required for the monitored concentration to reach

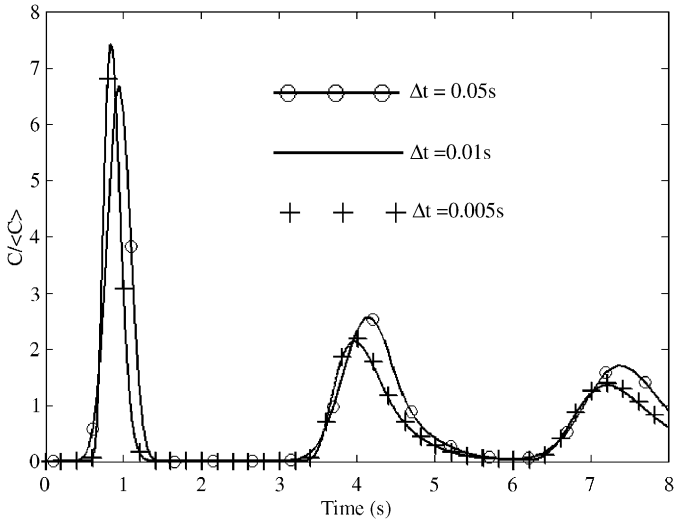

Fig. 8. Time evolution of the normalized concentration averaged on a given flow cross-section ($Z_{\text{imp}} = 0.25$): influence of the time step on the unsteady resolution (impeller 2, $N = 500$ rpm) (dots: numerical results; lines: best fit).

$\langle C \rangle$, with a threshold value of 5%, as summarized in Fig. 9 ($T_m = 37.7$ s is obtained in this example). Values of mixing time obtained for different conditions are shown as a function

of Reynolds number in Fig. 10. Mixing time decreases rapidly with the increase of Reynolds number (and thus impeller rotation speed), and only a weak influence of the impeller type is observed. The dimensionless mixing time $T_m^* = N.T_m$ is also presented. The evolution obtained is classical of a transition regime, that is characterized by a dependence of T_m^* to the Reynolds number, whereas, for high or low Reynolds number, T_m^* is found to be independent of the Reynolds number (Harnby et al., 1997). Curves evolution suggests that a fully turbulent flow regime tends to be achieved at $N > 400$ rpm (T_m^* is then almost constant). It is always difficult to compare mixing time between different geometries, because of the dependence of such a value to its measurement method (location of the injection, choice of the threshold concentration, etc.). A global comparison to mixing tanks is nevertheless interesting. As said before, T_m^* evolution is a function of the Reynolds number. Reynolds number definition is evidently different in mixing tank (there is no bulk velocity), and is given by $Re_m = \rho N D^2/\mu$. If N is ranged from $N = 250$ rpm to $N = 900$ rpm, the definitions give corresponding values from 3700 to 17 000 for Re (based on U_0 previous results), and 6600–24 000 for Re_m (with $D = L_y = 0.04$ m). It can be noticed that, in stirred tanks, transition regime is supposed for $10 < Re_m < 10^4$. The comparison of T_m^* values with classical results achieved in stirred tanks shows that the torus reactor seems a little less efficient than stirred tanks equipped with turbine, where T_m^* values are in the range of 80–100 (Norwood and Metzner, 1960). When marine impellers type are employed in stirred tanks, T_m^* can increase to values from 200 to 1000, as obtained in this study. Despite no remarkable improvement can be concluded using the torus geometry with respect to mixing time, there is also no important loss of efficiency. In the scope of PBR application, it is interesting to consider mixing time with regard to the mixing of a possible nutrient supply in the medium, as in the case of fed-batch or continuous cultures. Punctual feeding of nutrient and the punctual injection simulated are indeed almost similar. The maximum value of mixing time achieved is in the range of 90 s. This can be considered sufficiently short to have rapid homogenization of concentration in the reactor, whatever is the hydrodynamic condition applied (rotation speed or impeller type). This is especially verified for photosynthetic microorganisms which have low growth kinetics, with generation time of several hours. This will justify for future PBR modeling the common assumption of a well-mixed culture medium, and thus an homogeneous concentration of nutrients in the reactor.

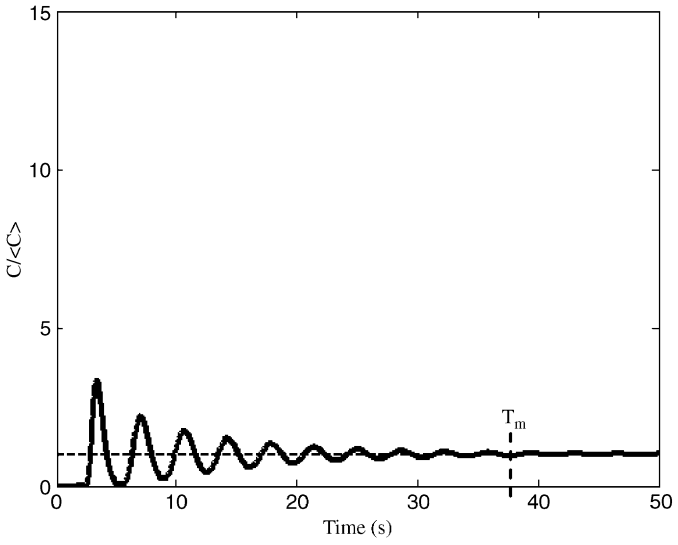

Fig. 9. Example of mixing time determination: time evolution of the normalized concentration averaged on the monitored surface ($Z_{imp} = 0.25$) (impeller 1, $N = 400$ rpm).

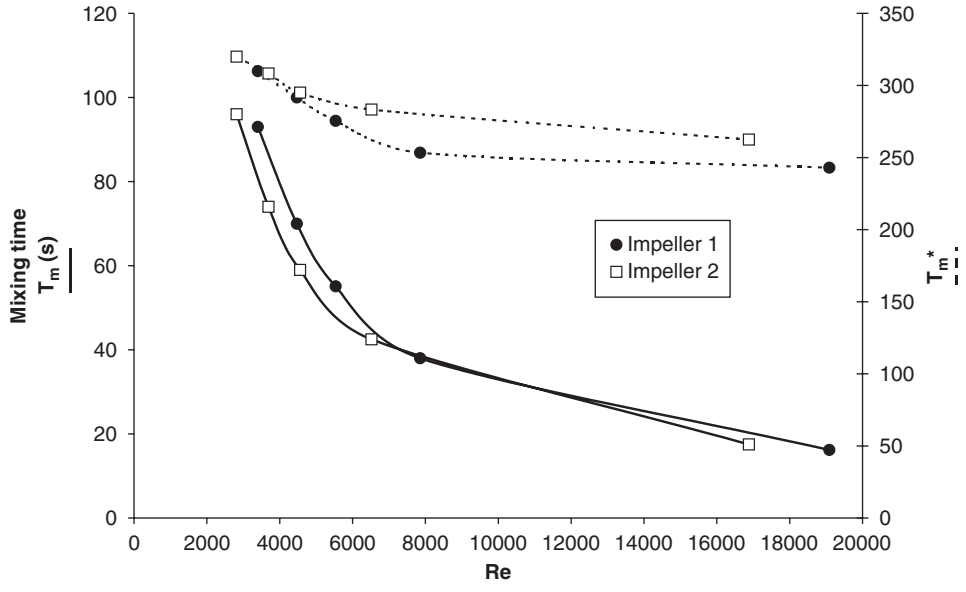

Fig. 10. Mixing time numerical results (dots: numerical results; lines: best fit).

4.3. Investigation of the lateral dispersion

In the field of photosynthetic microorganisms cultivation, mixing along the light gradient is of critical relevance. It can be investigated in details by determining the lateral dispersion (y-direction) of a passive tracer along one revolution of the torus reactor. The tracer injection was located in the same plane as before ($z/L_z = 0.25$). To investigate the lateral dispersion as a function of the axial distance from the injection (z-coordinate), tracer injection must be set along a line at y-constant value (Wen and Fan, 1974). This line is represented in Fig. 7 (central position in the gap width of the channel). For such an investigation, a time resolution of the tracer transport is not necessary (Eq. (3) is thus solved in steady state). For this, the tracer concentration in the injection is maintained constant (step type injection). Because of the loop configuration of the torus, tracer concentration in the position immediately preceding the injection must be imposed to null value, to prevent from perturbation of the injection condition due to tracer recirculation. An example of dispersion achieved is given in Fig. 7.

To relate the evolution of the tracer concentration to the lateral dispersion, a criterion ψ_y representing the spatial heterogeneity of tracer concentration C along the lateral distance y was defined. For a given cross-section located at the distance from the injection Z_{inj} (injection distance normalized with respect to the torus length L_z), the averaged concentration achieved is given by

$$\overline{\overline{C_{xy}(Z_{\text{inj}})}} = \frac{1}{L_x - L_y} \int_0^{L_y} \int_0^{L_x} C(x, y, Z_{\text{inj}})\, \mathrm{d}x\, \mathrm{d}y, \tag{4}$$

where L_x and L_y are torus channel dimension (because of the square section, $L_x = L_y$).

To determine lateral heterogeneity, it is necessary to calculate the averaged concentration obtained at a given lateral position y in the cross-section, that gives

$$\overline{C_x(y, Z_{\text{inj}})} = \frac{1}{L_x} \int_0^{L_x} C(x, y, Z_{\text{inj}})\, \mathrm{d}x. \tag{5}$$

An example of spatial evolution of $\overline{C_x(y, Z_{\text{inj}})}/\langle C \rangle$ is given in Fig. 11 (impeller 1, $N = 400$ rpm).

The root mean square of concentration variation along y-distance is then determined:

$$\sigma_y^2(Z_{\text{inj}}) = \frac{1}{L_y} \int_0^{L_y} (\overline{C_x(y, Z_{\text{inj}})} - \overline{\overline{C_{xy}(Z_{\text{inj}})})^2\, \mathrm{d}y. \tag{6}$$

Finally, criterion ψ_y is given by

$$\psi_y(Z_{\text{inj}}) = \frac{\sigma_y(Z_{\text{inj}})}{\sigma_y(Z_{\text{inj}} = 0)}. \tag{7}$$

To investigate influence of the particular flow generated in the torus geometry, the lateral dispersion was determined in a straight duct of similar square section as the torus reactor, leading to a pure axial flow. Inlet conditions were chosen in order to give established flow conditions, with the same mean bulk velocity U_0 as the one corresponding to a given impeller rotation in the torus reactor. The same procedure for numerical prediction as in the torus case was applied.

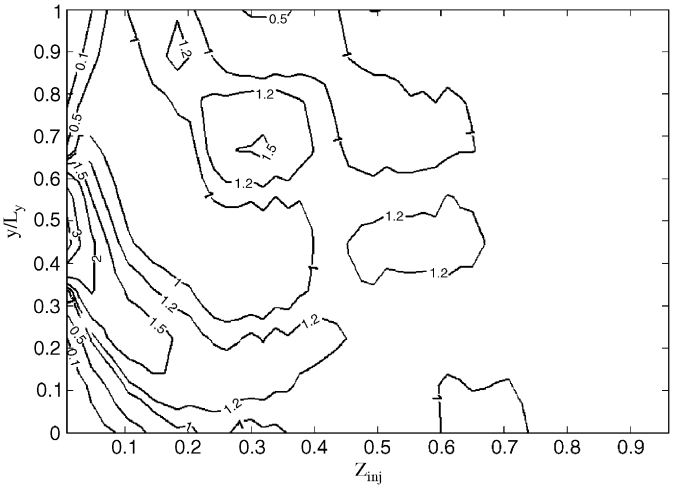

Fig. 11. Lateral dispersion investigation: example of $\overline{C_x}/\langle C \rangle$ spatial distribution (impeller 1, $N = 400$ rpm).

In the case of straight ducts, results of ψ_y are presented only for $U_0 = 0.085\,\mathrm{m\,s^1}$ and $U_0 = 0.477\,\mathrm{m\,s^{-1}}$, corresponding to mean bulk velocities achieved in the torus reactor with impeller 1 for $N = 200$ and 900 rpm, respectively (results of ψ_y for other impeller rotation speeds being included in this interval). In Fig. 12(a) and (b), results are given for impellers 1 and 2 for $N = 200$, 400 and 900 rpm. Results for $N = 300$ and 500 rpm are presented in Fig. 12(c).

For all simulations, a similar behavior is observed, with two characteristic parts, a first one with a rather regular decrease of the lateral heterogeneity in concentration, followed by a sudden drop for several order of magnitude when crossing the impeller region ($Z_{\text{inj}} = 0.75$). If the first part is considered, some interesting points are emphasized. For example, for impeller 2, the lateral dispersion is better for low values of the impeller rotation speed, a similar mixing efficiency being achieved as in the straight duct for $N > 500$ rpm. Such a result agrees with previous investigation of classical torus reactor (Pruvost et al., 2004a,c), where an increase in the impeller rotation speed has shown a complex influence on the resulting flow, due to the dual effect of marine impeller on axial flow circulation and swirl generation. If the impeller rotation speed is too high, a faster decrease of the swirl motion is observed, explained by Dean vortices appearance involved by higher centrifugal forces generated by a high flow circulation in the curved torus geometry. This explains the loss of efficiency on lateral dispersion for $N = 900$ rpm. Explanations with regard to flow structure will be presented later. By comparing both impellers, it again appears that impeller 1 gives rise to an enhancement of lateral mixing. Even for high rotation speeds of the impeller, results are always better than in a straight duct. It can be noticed that the evolution of the concentration heterogeneity ψ_y with the axial distance is less regular than for impeller 2. As it will be seen in foregoing figures, this is explained by a more complex resulting flow-field in the case of impeller 1, leading to a better mixing.

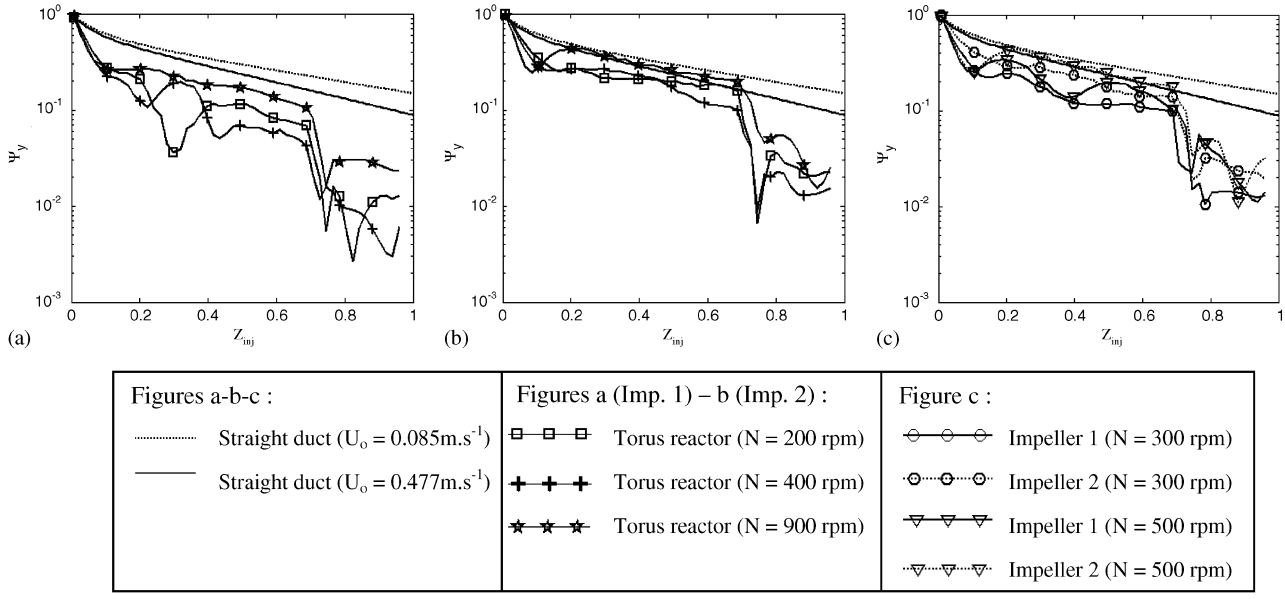

Fig. 12. Evolution of the concentration heterogeneity criterion ψ_y as a function of the injection distance (left: impeller 1; center: impeller 2; right: comparison between both impellers) (dots: numerical results; lines: best fit).

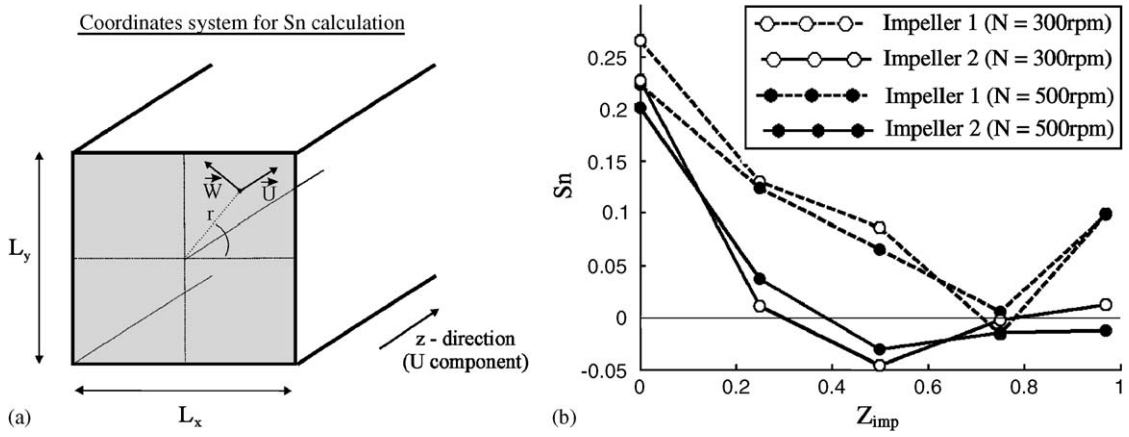

Fig. 13. (a) Coordinate system for Sn calculation and (b) Sn evolution as a function of impeller distance.

In a previous study of torus reactor (Pruvost et al., 2004a,c), it was found that the resulting flow in the geometry was correlated to a characteristic value of swirling flow, the swirl number Sn that represents the relative intensity between the swirling and the axial motion. Both swirl and axial pumping effects of the impeller are thus considered in Sn definition, leading to suitable value for torus reactor flow characterization. Calculation of Sn involves to determine the circumferential velocity W representing the swirl motion that decay along the z-axis. For a given cross-section S at constant z, Sn is given by

$$\mathrm{Sn} = \frac{\iint_S r U W \,\mathrm{d}S}{(L_y/2)\iint_S U^2 \,\mathrm{d}S}, \tag{8}$$

where U, is the mean axial velocity component (z-direction), W the circumferential one, r the radial distance from the z-axis, and S the surface of the cross-section considered (Fig. 13(a)).

Evolution of the swirl number with z-direction is given in Fig. 13(b) for both impellers, and for $N = 300$ and 500 rpm (similar conclusions are obtained for other rotation speeds). Results are presented as a function of the normalized distance from the impeller Z_{imp}. The decay of the swirl intensity is clearly shown. Initial value of Sn are around Sn = 0.2–0.27, and are only poorly influenced by N, which is a characteristic of marine type impeller effects in the loop configuration of the torus geometry, higher values of N leading to an equivalent increase in the axial and swirl motion (Pruvost et al., 2004c). In contrary, the swirl intensity decay is very different for both impellers. Impeller 2 shows a fast decrease with the impeller distance, around null values of Sn being observed for the most part of the reactor (60%). For impeller 1, the decay is sufficiently

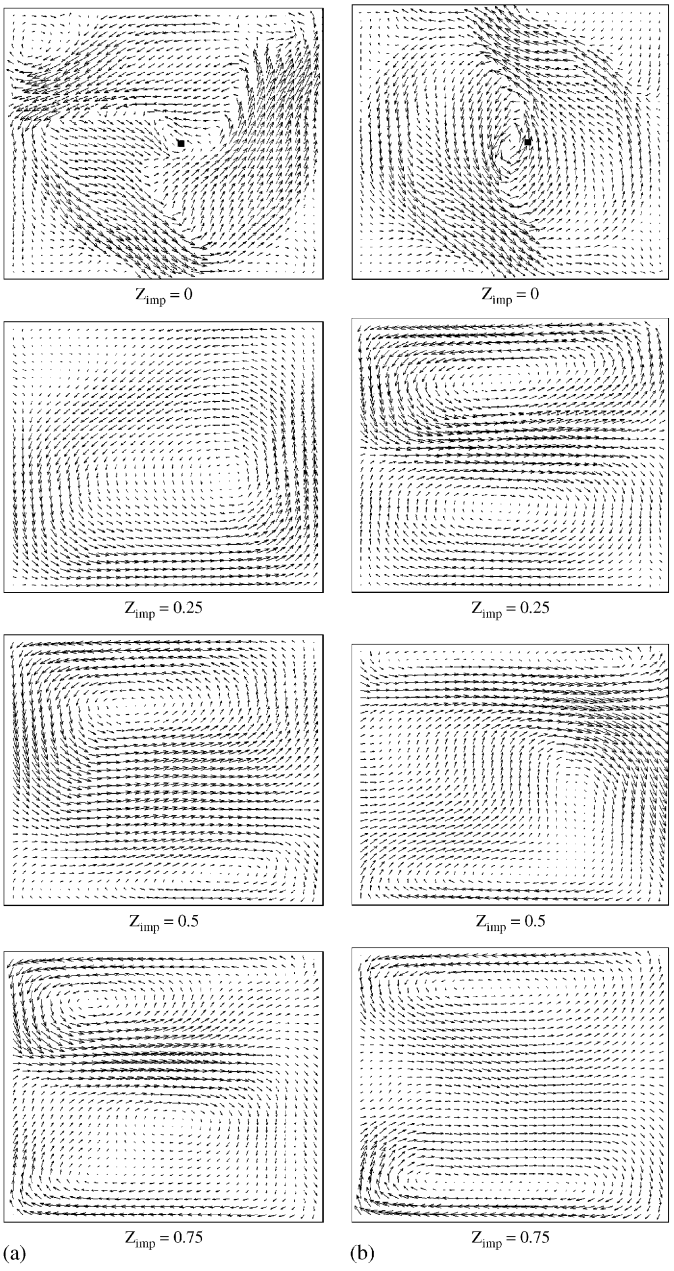

Fig. 14. Evolution of the flow structure in various cross-sections for $N = 300$ rpm (left: impeller 1; right: impeller 2).

low to conserve a non-negligible swirl intensity for almost all the reactor. Null values of Sn are only achieved at an upstream distance from the impeller of 0.75, but due to proximity of the impeller (after a complete loop), the swirl intensity again increases. It can be noticed that, for both impellers, evolutions of Sn are almost independent of the impeller rotation speed. Because Sn evolution is highly correlated to the resulting flow in the torus reactor (Pruvost et al., 2004c), the flow structure might remain rather unchanged when modifying N for a given impeller. In contrary, variations observed between both types of impellers would lead to different hydrodynamics.

To verify this, the flow structure is represented in Fig. 14 by plotting velocity-fields in different cross-sections for different axial distances from the impeller ($N = 300$ rpm). The complex rotating motion generated by both impellers is clearly observed at $Z_{\text{imp}} = 0$. If further positions are considered, two distinctive behaviors are observed. For impeller 2, well-known counter-rotating Dean vortices appears rapidly. For impeller 1, except at a distance from the impeller of 0.75, a solid body rotation is dominating. This is in perfect agreement with Sn evolutions. Same conclusions are achieved for others impeller rotation speeds (data not shown). These results illustrate again the particular flow-field involved in torus geometry, which is a complex interaction between the main rotating motion generated by the marine impeller, and Dean vortices that appear due to the bend curvature of the torus. In Pruvost et al. studies (Pruvost et al., 2004a,c), it was concluded to the pertinence of a threshold value for Sn of 0.2 to characterize competition between both phenomena. When the swirl number falls below this value, the swirl rotating motion is sufficiently weak to allow Dean vortices to appear. This is again observed in these results. Because the initial swirl intensity is around this threshold value, a perfect solid body rotation is never achieved, even in the vicinity of the impeller. In a given cross-section, both rotating motion and perturbations due to Dean vortices coexist, with more or less intensity depending on the distance from the impeller and of the impeller type.

If results on the flow-field structure and Sn evolution are now compared to the lateral dispersion prediction, a perfect correlation is observed. The lateral dispersion in the torus PBR is indeed directly linked to the resulting flow, and the swirl motion revealed to be of critical relevance. For example, fluctuations of ψ_y with the injection distance (Z_{inj} around 0.25) as observed in Fig. 12 (impeller 1, $N < 400$ rpm) are explained by the displacement of the center of the swirl motion along y-direction, as shown in Fig. 14. Better lateral mixing being achieved with impeller 1, it appears more interesting to promote a swirl motion in the PBR than Dean vortices. Global performance on a single loop of the torus geometry can by this way be improved. However, lateral dispersion results have shown that, whatever is the mixing achieved, an important dispersion of several order of magnitude is attained when crossing the impeller region. In the geometry under study, the loop configuration of the reactor induces a recirculating time below 10 s (10 s being obtained at $N = 200$ rpm). It can thus be concluded that, for photosynthetic microorganisms application, the torus PBR will give rise to a very efficient mixing, in particular along the light gradient, and in any case sufficient considering the slow growth kinetics of those microorganisms (doubling time of several hours).

5. Conclusion

The flow-field generated in a PBR of torus geometry has been investigated. A commercial code was used for this purpose, and predictions were validated with PIV measurements. In the field of photosynthetic microorganisms application, various relevant values were calculated, like mean bulk velocity U_0 related to cells sedimentation, averaged velocity component V_y reflecting light access conditions or averaged shear-stress $\langle\varepsilon\rangle$, a

criteria that should be adapted to cell fragility. Such determinations will serve as a basis for further investigation of the PBR, especially to determine the operating domain for a given cells cultivation, and to relate process conditions to the physiological response. In the field of PBR optimization, a comparison was made between two types of impellers. If species cultivated are not stress-sensitive (in the range of shear-stress intensities involved in the reactor), all of the investigations conclude to the interest of a classical three blades marine impeller (impeller 1), a more efficient flow circulation and mixing being achieved. If not the case, a compromise must be found based on the presented results and complementary experiments on living media.

Obtained results have shown in addition the relevance of the torus geometry to conduct photosynthetic microorganisms for the purpose of bioprocess modeling. By determining the lateral dispersion using numerical tracing methods, it was for example concluded to the great efficiency of such geometry in terms of mixing along the light attenuation coordinate, which is an important condition to allow an accurate modeling of the microorganisms photosynthetic growth. Indeed, in bioprocess modeling, it is often supposed an homogeneity in the overall biomass behavior. Such an assumption is valid in PBR modeling if all cells have a sufficient light access to consider all individuals cells responses identical without great deviation. This implies an effective mixing along the light gradient in the culture, that is allowed by the torus geometry. Combining this particularity with a square-channel and a plane illuminated surface, the torus PBR permits a high degree of control of the light received in the reactor. Such a geometry appears thus as an alternative, but pertinent, solution in the field of photosynthetic microorganisms studies.

Notation

C_j	passive tracer concentration (Eq. (3)), mol m^{-3}
D_j	laminar mass diffusivity of the passive tracer, m^2 s^{-1}
D_{jt}	turbulent mass diffusivity of the passive tracer, m^2 s^{-1}
k	turbulent kinetic energy, m^2 s^{-2}
L_x	gap width of the torus photobioreactor, m
L_y	photobioreactor depth ($L_x = L_y$), m
L_z	length of the torus photobioreactor, m
N	rotation velocity of the impeller, rpm
R_c	external torus photobioreactor radius, m
$Re = \rho U_0 L_y/\mu$	Reynolds number
$Re_m = \rho N D^2/\mu$	Reynolds number (definition used for mixing tank, with $L_y = D$)
S	rate-of-deformation tensor (Eq. (1)), s^{-1}
S_{ct}	turbulent Schmidt number (Eq. (2))
Sn	swirl number (Eq. (8))
T_m	mixing time, s
T_m^*	dimensionless mixing time
U	mean axial velocity component, m s^{-1}
$U_0 = Q/(L_x.L_y)$	mean bulk velocity, m s^{-1}
V_y	velocity component along the light gradient (y-coordinate),m s^{-1}
y	distance along light gradient direction, m
z	longitudinal coordinate, m
Z_{inj}	normalized distance from the injection
Z_{imp}	normalized distance from the impeller

Greek letters

ε	strain rate (Eq. (1)), s^{-1}
ε_{imp}	strain rate in the impeller region, s^{-1}
μ	dynamic viscosity of water, Pa s
μ_t	turbulent viscosity, Pa s
ψ_y	criterion of spatial heterogeneity of tracer concentration along y-distance (Eq. (7))

Other symbol

$\langle\,\rangle$	spatial averaging

References

Barbosa, M.J., Hadiyanto, Wijffels, R.H., 2004. Overcoming shear stress of microalgae cultures in sparged photobioreactors. Biotechnology and Bioengineering 85 (1), 78–85.

Bird, R.B., Stewart, W.E., Lightfoot, E.N., 2002. Transport Phenomena. Second ed. Wiley, New York.

Brucato, A., Ciofalo, M., Grisafi, F., Micale, G., 1998. Numerical prediction of flow-fields in baffled stirred vessels: a comparison of alternative modelling approaches. Chemical Engineering Science 53 (21), 3653–3684.

Chini Zitelli, G.C., Pastorelli, R., Tredici, M.R., 2000. A modular flat panel photobioreactor (MFPP) for indoor mass cultivation of *Nannochloropsis* sp. under artificial illumination. Journal of Applied Phycology 12 (3–5), 521–526.

Cornet, J.F., Albiol, J., 2000. Modeling photoheterotrophic growth kinetics of *Rhodospirillum rubrum* in rectangular photobioreactors. Biotechnology Progress 16, 199–207.

Cornet, J.F., Dussap, C.G., Gros, J.B., 1994. Conversion of radiant light energy in photobioreactors. A.I.Ch.E. Journal 40 (6), 1055–1066.

Cornet, J.F., Dussap, C.G., Gros, J.B., 1995. A simplified monodimensional approach for modeling coupling between radiant light transfer and growth kinetics in photobioreactors. Chemical Engineering Science 50 (9), 1489–1500.

Cornet, J.F., Dussap, C.G., Gros, J.B., 1998. Kinetics and energetics of photosynthetic micro-organisms in photobioreactors: application to *Spirulina* growth. Advances in Biochemical Engineering and Biotechnology 59, 155–224.

Cornet, J.F., Favier, L., Dussap, C.G., 2003. Modeling stability of photoheterotrophic continuous cultures in photobioreactors. Biotechnology Progress 19 (4), 1216–1227.

Csogör, Z., Herrenbauer, M., Perner, I., Schmidt, K., Posten, C., 1999. Design of a photobioreactor for modelling purposes. Chemical Engineering and Processing 38, 517–523.

Csogör, Z., Herrenbauer, M., Schmidt, K., Posten, C., 2001. Light distribution in a novel photobioreactor—modelling for optimization. Journal of Applied Phycology 13, 325–333.

Curran, S.J., Black, R.A., 2004. Quantitative experimental study of shear stresses and mixing in progressive flow regimes within annular-flow bioreactors. Chemical Engineering Science 59 (24), 5859–5868.

Elias, C.B., Desai, R.B., Patole, M.S., Joshi, J.B., Mashelkar, R.A., 1995. Turbulent shear stress—effect on mammalian cell culture and measurement using laser Doppler anemometer. Chemical Engineering Science 50 (15), 2431–2440.

Ghadge, R.S., Patwardhan, A.W., Sawant, S.B., Joshi, J.B., 2005. Effect of flow pattern on cellulase deactivation in stirred tank bioreactors. Chemical Engineering Science 60, 1067–1083.

Grobbelaar, J.U., Nebdal, L., Tichy, V., 1996. Influence of high light/dark fluctuations on photosynthetic characteristics of microalgae photoacclimated to different light intensities and implications for mass algal cultivation. Journal of Applied Phycology 8, 335–343.

Harnby, N., Edwards, M.F., Nienow, A.W., 1997. Mixing in the Process Industries. Butterworth Heinemann, London.

Hoekema, S., Bijmans, M., Janssen, M., Tramper, J., Wijffels, R.H., 2002. A pneumatically agitated flat-panel photobioreactor with gas re-circulation: anaerobic photoheterotrophic cultivation of a purple non-sulfur bacterium. International Journal of Hydrogen Energy 27 (11–12), 1331–1338.

Janssen, M.G.J., Kuijpers, T.C., Veldhoen, B., Ternbach, M.B., Tramper, J., Mur, L.R., Wijffels, R.H., 1999. Specific growth rate of *Chlamydomonas reinhardtii* and *Chlorella sorokiniana* under medium duration light/dark cycles 13–87 s. Journal of Biotechnology 70, 323–333.

Jaouen, P., Vandanjon, L., Quèmèneur, F., 1999. The shear stress of microalgal cell suspensions (*Tetraselmis suecica*) in tangential flow filtration systems: the role of pumps. Bioresources Technology 68, 149–154.

Khalid, A., Legrand, J., 2001. Energy dissipation distribution and mixing in a torus reactor. Chemical Engineering Communications 185, 141–164.

Lee, K., Lee, C.G., 2001. Effect of light/dark cycles on wastewater treatments by microalgae. Biotechnology and Bioprocess Engineering 6, 194–199.

Legrand, J., Guéguen, J., Berot, S., Popineau, Y., Nouri, L., 1997. Acetylation of pea isolate in a torus microreactor. Biotechnology and Bioengineering 53 (4), 410–414.

Lorenz, R.T., Cysewski, G.R., 2000. Commercial potential for *Haematococcus* microalgae as a natural source of astaxanthin. Trends in Biotechnology 18 (4), 160–167.

Luo, H.P., Al-Dahhan, M.H., 2004. Analyzing and modeling of photobioreactors by combining first principles of physiology and hydrodynamics. Biotechnology and Bioengineering 85 (4), 382–393.

Luo, H.P., Kemoun, A., Al-Dahhan, M.H., Fernandez Sevilla, J.M., Garcia Sanchez, J.L., Garcia Camacho, F., Molina Grima, E., 2003. Analysis of photobioreactors for culturing high-value microalgae and cyanobacteria via an advanced diagnostic technique: CARPT. Chemical Engineering Science 58 (12), 2519–2527.

Merchuk, J.C., Ronen, M., Giris, S., Arad, S., 1998. Light/dark cycles in the growth of the red microalga *Porphyridium sp*. Biotechnology and Bioengineering 59 (6), 705–713.

Muller-Feuga, A., Le Guedes, R., Pruvost, J., 2003a. Benefits and limitations of modeling for optimization of *Porphyridium cruentum* cultures in an annular photobioreactor. Journal of Biotechnology 103 (2), 153–163.

Muller-Feuga, A., Pruvost, J., Le Guedes, R., Le Dean, L., Legentilhomme, L., Legrand, J., 2003b. Swirling flow implementation in a photobioreactor for batch and continuous cultures of *Porphyridium cruentum*. Biotechnology and Bioengineering 84 (5), 544–551.

Norwood, K.W., Metzner, B., 1960. Flow patterns and mixing rates in agitated vessels. A.I.Ch.E. Journal 6, 432–437.

Nouri, L., Legrand, J., Popineau, Y., Belleville, P., 1997. Enzymatic hydrolysis of wheat proteins. Part II. Comparison of performance of batch-stirred and torus reactors. Chemical Engineering Journal 65, 195–199.

Ogbonna, J.C., Yada, H., Masui, H., Tanaka, H., 1996. A novel internally illuminated stirred tank photobioreactor for large-scale cultivation of photosynthetic cells. Journal of Fermentation and Bioengineering 82 (1), 61–67.

Olaizola, M., 2003. Commercial development of microalgal biotechnology: from the test tube to the marketplace. Biomolecular Engineering 20 (4–6), 459–466.

Pottier, L., Pruvost, J., Deremetz, J., Cornet, J.F., Legrand, J., Dussap, C.G., 2005. A fully predictive model for one-dimensional light attenuation by *Chlamydomonas reinhardtii* in a torus reactor. Biotechnology and Bioengineering 91 (5), 569–582.

Pruvost, J., Legrand, J., Legentilhomme, P., Muller-Feuga, A., 2002. Simulation of microalgae growth in limiting light conditions—flow effect. A.I.Ch.E. Journal 48, 1109–1120.

Pruvost, J., Legrand, J., Legentilhomme, P., 2004a. Numerical investigation of bend and torus flows. Part I. Effect of swirl motion on flow structure in U-bend. Chemical Engineering Science 59 (16), 3345–3357.

Pruvost, J., Legrand, J., Legentilhomme, P., Muller-Feuga, A., 2004b. Effect of inlet type on deformation stress-fields and mixing in annular turbulent swirling decaying flows. Canadian Journal of Chemical Engineering 82, 495–503.

Pruvost, J., Legrand, J., Legentilhomme, P., Rosant, J.M., 2004c. Numerical investigation of bend and torus flows. Part II. Flow simulation in torus reactor. Chemical Engineering Science 59 (16), 3359–3370.

Pulz, O., 2001. Photobioreactors: production systems for phototrophic microorganisms. Applied Microbiology and Biotechnology 57 (3), 287–293.

Richmond, A., 2004. Principles for attaining maximal microalgal productivity in photobioreactors: an overview. Hydrobiologia 512, 33–37.

Sanchez Miron, A., Ceron Garcia, M.C., Contreras Gomez, A., Garcia Camacho, F., Molina Grima, E., Chisti, Y., 2003. Shear stress tolerance and biochemical characterization of *Phaeodactylum tricornutum* in quasi steady-state continuous culture in outdoor photobioreactors. Biochemical Engineering Journal 16 (3), 287–297.

Tanaka, M., O'Shima, E., 1988. Dispersing behavior of droplets in suspension polymerization of styrene in a loop reactor. Canadian Journal of Chemical Engineering 66, 29–35.

Tredici, M.R., Materassi, R., 1992. From open ponds to vertical alveolar panels: the Italian experience in the development of reactors for the mass cultivation of phototrophic microorganisms. Journal of Applied Phycology 4 (3), 221–231.

Wen, C.Y., Fan, L.T., 1974. Models for Flow Systems and Chemical Reactors. Series CPaE. Marcel Dekker, New York.

Wilcox, D.C., 1998. Turbulence Modeling for CFD. DCW Industries, La Canada, California.

Wu, X., Merchuk, J.C., 2001. A model integrating fluid dynamics in photosynthesis and photoinhibition processes. Chemical Engineering Science 56, 3527–3538.

Wu, X., Merchuk, J.C., 2002. Simulation of algae growth in an bench-scale column reactor. Biotechnology and Bioengineering 80 (2), 156–168.